Monthly Notices of the ROYAL ASTRONOMICAL SOCIETY
MNRAS **499,** L16–L20 (2020) doi:10.1093/mnrasl/slaa148

Detection of 15 bursts from the fast radio burst 180916.J0158+65 with the upgraded Giant Metrewave Radio Telescope

V. R. Marthi [1]★ T. Gautam,[2] D. Z. Li [2,3,4] H-H. Lin,[2,3] R. A. Main,[2]★ A. Naidu,[5,6] U-L. Pen[2,3,7,8,9] and R. S. Wharton[2]★

[1]*National Centre for Radio Astrophysics, Tata Institute of Fundamental Research, Post Bag 3, Ganeshkhind, Pune - 411 007, India*
[2]*Max-Planck-Institut für Radioastronomie, Auf dem Hügel 69, D-53121 Bonn, Germany*
[3]*Canadian Institute for Theoretical Astrophysics, 60 St George Street, Toronto, ON M5S 1A7,Canada*
[4]*Department of Physics, University of Toronto, 60 St George Street, Toronto, ON M5S 1A7, Canada*
[5]*Department of Physics, McGill University, 3600 rue University, Montréal, QC H3A 2T8, Canada*
[6]*Oxford Astrophysics, Denys Wilkinson Building, Keble Road, Oxford, OX1 3RH*
[7]*Dunlap Institute for Astronomy and Astrophysics, University of Toronto, 50 St George Street, Toronto, ON M5S 3H4, Canada*
[8]*Program in Cosmology and Gravitation, Canadian Institute for Advanced Research, Toronto, ON M5G 1Z8, Canada*
[9]*Perimeter Institute for Theoretical Physics, 31 Caroline Street North, Waterloo, ON N2L 2Y5, Canada*

Accepted 2020 August 24. Received 2020 August 21; in original form 2020 July 28

ABSTRACT

We report the findings of an upgraded Giant Metrewave Radio Telescope (uGMRT) observing campaign for FRB 180916.J0158+65, which was recently found to show a 16.35-d periodicity of its active cycle. We observed the source at 550–750 MHz for ∼2 h during each of three successive cycles at the peak of its expected active period. We find 0, 12 and 3 bursts, respectively, implying a highly variable bursting rate even within the active phase. We consistently detect faint bursts with spectral energies only an order of magnitude higher than the Galactic burst source SGR 1935+2154. The times of arrival of the detected bursts rule out many possible aliased solutions, strengthening the findings of the 16.35-d periodicity. A periodicity search over a short time-scale returned no highly significant candidates. Two of the beamformer-detected bursts were bright enough to be clearly detected in the imaging data, achieving subarcsec localization, and proving to be a proof-of-concept for FRB imaging with the GMRT. We provide a 3σ upper limit of the persistent radio flux density at 650 MHz of 66 μJy, which, combined with the European VLBI Network and Very Large Array limits at 1.6 GHz, further constrains any potential radio counterpart. These results demonstrate the power of the uGMRT for providing targeted observations to detect and localize known repeating FRBs.

Key words: methods: observational – techniques: interferometric – radio continuum: transients; fast radio bursts.

1 INTRODUCTION

Since the discovery of fast radio bursts (FRBs) more than a decade ago (Lorimer et al. 2007), there has been considerable interest in their origin, which remains unknown still. The observed dispersion measures (DMs) of these bursts far exceed the expected contribution from the Milky Way, suggesting that FRBs are located at cosmological distances. Indeeed, sub-rcsecond localizations for five of the ∼100 known FRBs have placed them in host galaxies with redshifts $z = 0.03-0.66$ (Chatterjee et al. 2017; Bannister et al. 2019; Prochaska et al. 2019; Ravi et al. 2019; Marcote et al. 2020). A small subset of FRBs are seen to repeat, providing an excellent laboratory for understanding the physical mechanism that produces FRBs as we can conduct targeted observations that are not possible with any other FRB source.

FRB 180916.J0158+65 is the most active repeating source detected at 400–800 MHz by the Canadian Hydrogen Intensity Mapping Experiment (CHIME; Andersen et al. 2019), with 52 bursts reported as of 2020 July 20.[1] Recently, the European VLBI Network (EVN) localized it to a star-forming region in a spiral galaxy at $z = 0.0337$ ($D_L \approx 150$ Mpc; Marcote et al. 2020). This is by far the closest localized extragalactic FRB source, an order of magnitude closer than other localized sources.

Remarkably, a periodicity in the activity of FRB 180916.J0158+65 has recently been discovered. All CHIME-detected bursts occur within a 5-d window that repeats every 16.35 d (Amiri et al. 2020). This is the first detected periodicity in a repeating FRB and presents a unique opportunity to unveil the nature of FRB sources. The periodicity could be caused by the orbital motion of the FRB source around a companion (Dai et al. 2016; Ioka & Zhang 2020; Lyutikov, Barkov & Giannios 2020), by the precession of the burst emitting object itself (Levin,

★ E-mail: vrmarthi@ncra.tifr.res.in (VRM); ramain@mpifr-bonn.mpg.de (RAM); wharton@mpifr-bonn.mpg.de (RSW)

[1] https://www.chime-frb.ca/repeaters

Beloborodov & Bransgrove 2020; Yang & Zou 2020; Zanazzi & Lai 2020) or ultralong rotational periods (Beniamini, Wadiasingh & Metzger 2020). Rajwade et al. (2020) have similarly detected a tentative ∼157-d periodicity in FRB 121102, an order of magnitude larger. The ability to predict the next active phase of the repeating FRB 180916.J0158+65 means that highly efficient follow-up observations can be conducted with sensitive radio telescopes. Thus, regular monitoring observations can be crucial in pinning down the FRB emission mechanism, and especially in bridging the energy gap with Galactic radio transient counterparts. Also, they can help us understand the origin of its periodicity.

Here we present the findings from observations of FRB 180916.J0158+65 during three successive active windows taken as part of an ongoing monitoring campaign with the upgraded Giant Metrewave Radio Telescope (uGMRT; Gupta et al. 2017). This letter is organized as follows. In Section 2, we describe our observations, data reduction and burst search methods. In Section 3, we detail our results, including our detected bursts, a periodicity search over a short time-scale, resolving aliasing ambiguities in the 16.35-d periodicity, burst localizations and limits on the flux of the persistent source. Finally, Section 4 contains our concluding remarks.

2 OBSERVATIONS

The uGMRT observations were carried out on 2020 March 09, 2020 March 24, and 2020 June 30, all near the peak of the active phase within the 16.35-d period. We used the uGMRT Band-4 receiver at 550–750 MHz, a subset of the CHIME band. The GMRT Wideband Backend (GWB; Reddy et al. 2017) was deployed in the 200-MHz 8-bit beamformer mode. Interferometric visibilities from the same FX correlator were simultaneously recorded. In the beamformer mode of operation, the GWB is capable of computing four simultaneous independent beams. For our observations, we recorded the coherently dedispersed (CD) phased array beam. The correlator was set up to split the 200-MHz bandwidth into 2048 channels. The beam output was integrated to 327.68 μs, while the visibilities were integrated to 2.68 s.

In each session, we chose 0217+738, an unresolved radio source ∼10° away from our target, as the phase calibrator. We have a total of 110 min of exposure in each of the first two sessions and 85 min in the third.

2.1 Detecting the bursts

We performed a standard PRESTO (Ransom, Eikenberry & Middleditch 2002) search on the coherently dedispersed phased array data. We flagged RFI in 2-s windows using the `rfifind` algorithm, and used the `prepsubband` command to create dedispersed time series in 201 steps of 0.5 pc cm^{-3}, with the DM centred at 348.82 pc cm^{-3}. We searched for bursts using `single_pulse_search.py`, identifying candidates above 6σ, and distinguishing candidates from RFI by eye. On 2020 March 24, 2020 June 30 and 2020 March 09, 12, 3 and no bursts were detected, respectively, as shown in Fig. 1. The profiles and dynamic spectra of bursts 11 and 04, the brightest pair among those reported here, are shown in Fig. 2. The time of arrival (ToA) for each burst was obtained as the offset from the barycentred start time of the respective scan, returned by PRESTO.

2.2 Flux density calibration

On 2020 March 24, we also used our phase calibrator 0217+738, a flat spectrum 2-Jy source, as the flux calibrator. Therefore, we allow for a modest 30 per cent systematic uncertainty in the derived system-equivalent flux density (SEFD), included in the error bar of the fluence for each burst in Table 1.

However, on 2020 June 30, we observed 3C 147, a bright flux calibrator. Therefore, we absorb only a 10 per cent systematic uncertainty in the SEFD, again included in the fluences of those bursts. We find that the SEFD on the two days, and therefore the peak flux densities of bursts with similar signal-to-noise ratio (S/N) in the two sessions, are comparable, inspiring confidence in our calibration of the March 24 data.

Table 1 gives the ToA, along with the identifier number, the peak flux density, fluence and the error bar on the fluence for each burst.

3 RESULTS

3.1 DM optimization with the power spectrum

The burst profile obtained with a DM that maximizes the peak S/N is degenerate with any intrinsic temporal substructure. It is therefore more meaningful to maximize the temporal substructure, recognizing its importance for investigating emission models and mechanisms.

We have developed a new method to determine the optimal DM that maximizes energy in the substructure, with similar motivation to the substructure maximization developed for FRB 121102 (Hessels et al. 2019). First, we obtain the singular value decomposition (SVD) of the time-frequency burst profile. Next, we identify the signal-free modes in the SVD, using this to reconstruct the noise and subtract it from the input burst profile. Finally, we produce the power spectrum of the noise-subtracted burst profile for a range of DMs around the nominal value, examining the power in the highest noise-free frequency mode as a function of the DM. The peak and the width of the Gaussian fit to the power yield the DM that maximizes substructure. For three selected bursts (i.e. 04, 11 and 12), we obtain optimized DM values of 349.0 ± 0.3, 348.8 ± 0.1 and 348.9 ± 0.9 pc cm^{-3}, respectively, consistent with the nominal value of 348.82 pc cm^{-3} used throughout this work. The results of applying this technique to all the detected bursts will be detailed in a forthcoming paper (Lin et al., in preparation).

3.2 Energy scales

We detected bursts in a range of fluences between ∼0.1 and 48 Jy ms, the lower end of this range being comparable with the faintest burst (i.e. 0.2 Jy ms) detected with the EVN. Using the luminosity distance of 149.0 ± 0.9 Mpc (Marcote et al. 2020), the spectral energy of our faintest detected burst (assuming an isotropic source) is ∼2.7 ± 1.6 × 10^{27} erg Hz^{-1}.

Recently, the brightest known Galactic radio burst to date was detected by CHIME (Andersen et al. 2020) and STARE2 (Bochenek et al. 2020), originating from the Galactic magnetar SGR 1935+2154. With an isotropic-equivalent spectral energy release of 1.6 ± 0.3 × 10^{26} erg Hz^{-1} it is approaching the energy scales of FRBs at only a factor of ∼10 to 25 fainter than our faintest burst, possibly representing the Galactic counterpart of an FRB. Continuing to probe the faint end of the FRB energy distribution could bridge the gap between the brightest Galactic bursts and the faintest FRBs.

3.3 Resolving aliasing ambiguities in the 16.35-d periodicity

FRB 180916.J0158+65 stays in the CHIME/FRB field of view for tens of minutes every sidereal day. The beating of the CHIME/FRB regular exposure pattern with the intrinsic 16.35-d period leads to a degeneracy between frequency $f_0 = (P_0)^{-1} = (16.35\,\mathrm{d})^{-1}$ and

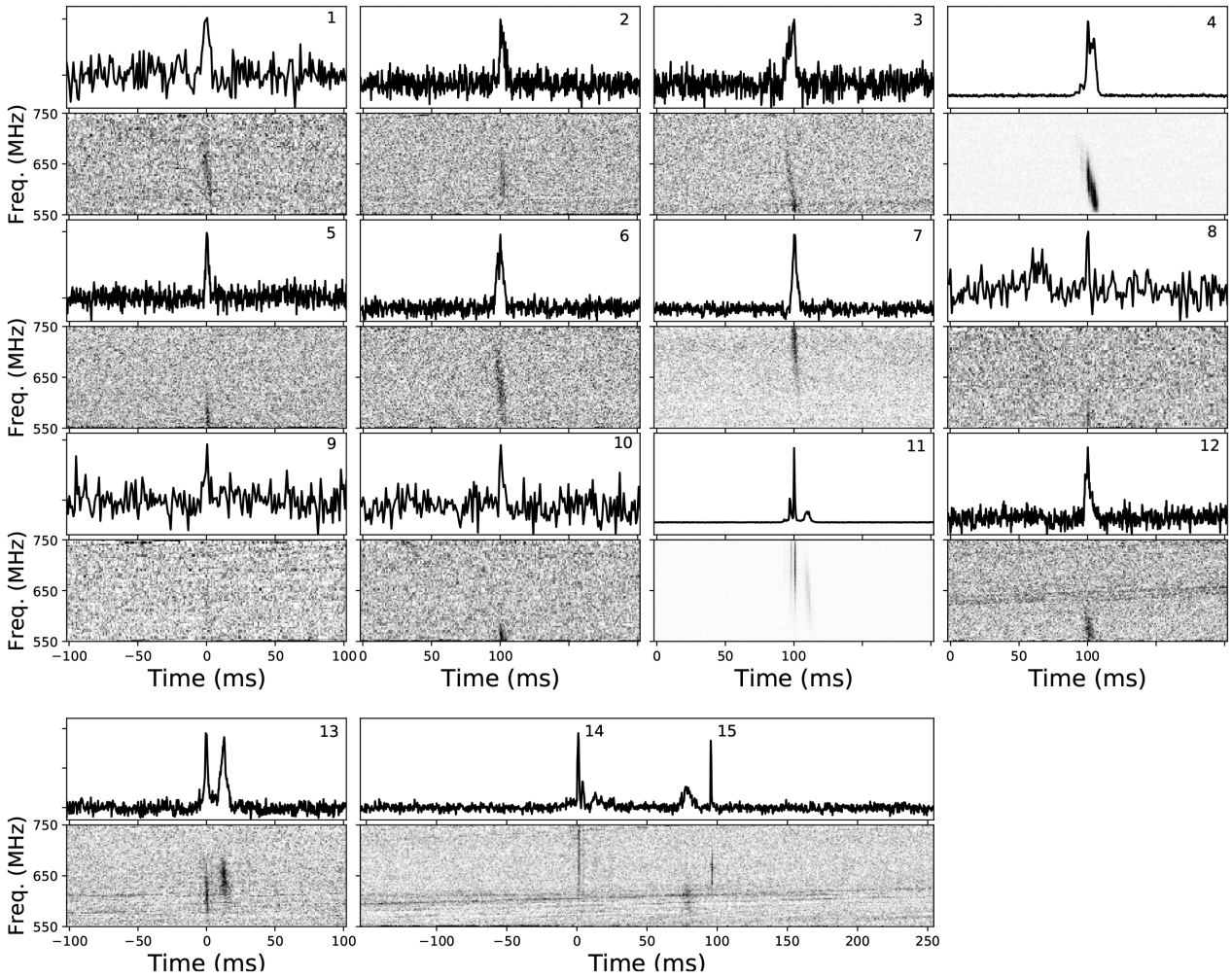

Figure 1. Dynamic spectra of all detected bursts, in sequential order. For plotting purposes, frequency was binned by a factor of 16. In bursts 1, 8, 9 and 10, frequency was binned by an additional factor of 2, and time by a factor of 3 to 983.04 μs. The top panels show our detections from March 24, while the panels in the bottom row are from June 30, where the final panel is interpreted as at least two separate bursts.

an alias $f_N = N\, f_{\rm sid} \pm f_0$, where N is an integer and $f_{\rm sid} = (0.99727\,{\rm d})^{-1}$ is the frequency of a sidereal day (Amiri et al. 2020). An upper limit on N can be estimated from the observed duty cycle over exposure time. With a 5/16.35-d fractional active phase and 12-min exposure per sidereal day ($\sim$0.008 sidereal day), $N_{\rm max} = 5/16.35/0.008 = 38$.

These aliasing ambiguities can be resolved using burst detections at other observatories, as they can observe during the inactive windows of the aliased solutions. Using the bursts detected by CHIME/FRB and all published bursts from other observatories, including the 15 described in this work, we fold at different alias periods. As shown in Fig. 3, the contiguous inactive fraction (Rajwade et al. 2020) is much smaller for all beating periods, compared with the 16.35-d period. This indicates that the bursts are falling outside the active window for the alias frequency, disfavouring the possibility of an aliased period being the real period.

3.4 Imaging

Using the interferometric visibilities that were simultaneously recorded, we can localize the brightest bursts and also search for any persistent radio emission associated with the FRB. The data of 2020 March 24 were processed and calibrated using the CASA software package (McMullin et al. 2007). We used 0217+738 as a complex gain calibrator.

Even though the time resolution of the visibility data was 2.68 s, two of the bursts from March 24 were bright enough for an imaging detection. As the dispersive delay across the band is only $\approx$2.2 s, we did not attempt to de-disperse the visibility data. For burst 04, we made an image from two time samples and, for burst 11, we made an image from one time sample of the calibrated visibility data. For each image, we also carried out one round of phase-only self-calibration on other bright sources in the field. Burst 04 was detected with S/N = 21 and burst 11 with S/N = 27. Both bursts could be localized to a 5σ positional uncertainty of $\lesssim 1$ arcsec. Although a precise localization has already been determined through very-long-baseline interferometry with the EVN for this source (Marcote et al. 2020), our results provide an interesting proof-of-concept for future subarcsec localizations with the GMRT. The instantaneous images of bursts 04 and 11 are shown in Fig. 4.

No source was detected at the FRB position in the image (see Fig. 4) made with the full $\sim$2-h observation on March 24, which allows us to set a 3σ upper limit on the flux density at 650 MHz of 66 μJy. Marcote et al. (2020) used the Very Large Array at 1.6 GHz to set a 3σ flux density limit of 18 μJy, which is more constraining than our result for spectral indices $\alpha > -1.4$.

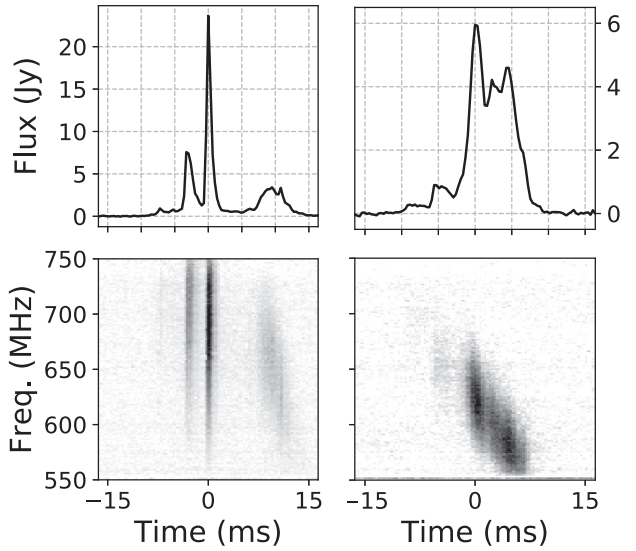

Figure 2. Zoomed-in dynamic spectra and profiles of burst 11 (left) and burst 04 (right). The greyscale scheme is in square root scaling to reveal the faint emission. While both bursts show clear substructure and multiple bright peaks, there is persistent detectable emission for the full ∼20-ms duration of the bursts.

Table 1. The ToA of the 15 bursts and their fluences. Only frequencies 569.5−745.4 MHz (channels 200–2000) were included for estimating the fluence.

Burst no.	Barycentric ToA	Peak flux (Jy)	Fluence (Jy ms)	Error (Jy ms)
	MJD 58932+			
01	0.542126	0.19	0.26	0.12
02	0.542939	0.32	0.65	0.23
03	0.544481	0.27	0.37	0.15
04	0.550594	5.98	32.90	9.91
05	0.557890	0.38	0.24	0.10
06	0.563082	0.57	1.54	0.50
07	0.567436	0.83	6.68	2.04
08	0.579496	0.21	0.12	0.06
09	0.580353	0.17	0.09	0.06
10	0.588714	0.21	0.10	0.06
11	0.604069	23.65	47.80	14.39
12	0.612024	0.57	3.86	1.20
	MJD 59030+			
13	0.297435	0.58	0.82	0.42
14	0.298753	0.80	6.63	0.74
15	0.298754	0.72	2.97	0.50

3.5 Periodicity search on small time-scales

We performed a Fourier domain acceleration search using the PRESTO `accelsearch` algorithm on the ∼2-h on-target data on 2020 March 24, in the DM range of 348.82 ± 5 pc cm^{-3} with periods between 1 ms to 20 s. The full data search was sensitive to accelerations up to ∼28 ms^{-2} for a periodicity of 10 ms, while 20-min segments of the data were also searched making the search sensitive to accelerations up to ∼200 ms^{-2}. In addition, we performed a jerk search (Andersen & Ransom 2018) to account for changing accelerations within the span of our observation.

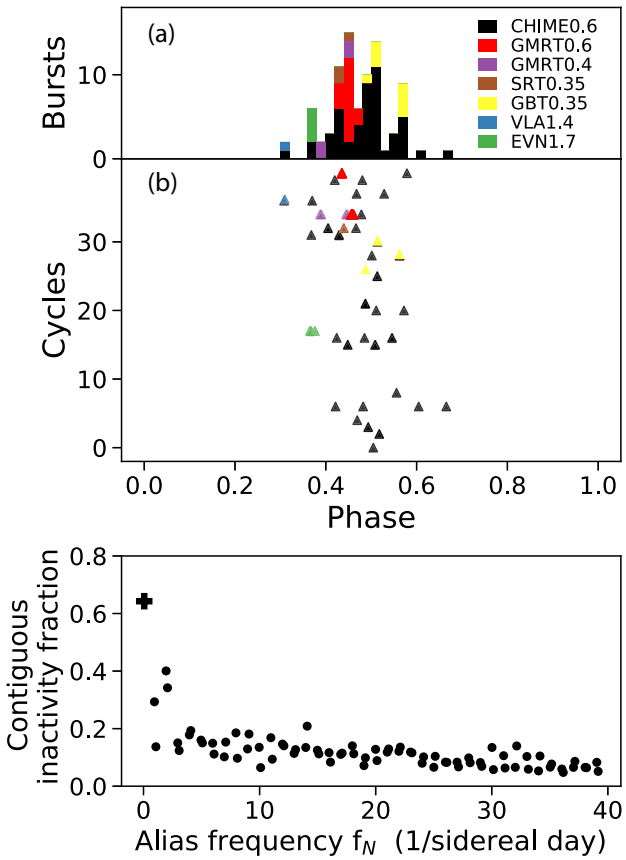

Figure 3. The top panel shows the ToA of bursts from FRB 180916.J0158+65 folded at a period of 16.35 d with MJD 58369.18 referenced as phase 0. Bursts captured by different facilities (Aggarwal et al. 2020; Amiri et al. 2020; Chawla et al. 2020; Marcote et al. 2020; Pilia et al. 2020; Sand et al. 2020) are shown in different colours as specified in the legend. The numbers in the legend are the central frequency of the observation in unit of GHz. (a) Number of bursts at each phase. (b) The phase of detection for individual cycles. The bottom panel shows the longest contiguous phase region without detectable activity for the plausible beat periods. The dark cross is for the 16.35-d periodicity.

A number of weak candidates have shown up in the search, including a 15.6-ms ($\sim 6\sigma$) periodicity candidate in one of the 20-min data segments. However, this periodicity is not detected with any significance when we search the full ∼2-h observation.

4 SUMMARY AND CONCLUSIONS

We have outlined the uGMRT detection of 15 bursts, of which 12 is the largest number of single-session detections, including the faintest ones to date. The burst rate appears to be highly variable and the faintest burst is only ∼10× brighter than the brightest Galactic burst detected to date.

We have effectively resolved aliasing ambiguities in the 16.35-d period. A survey telescope such as CHIME is well tuned to discovering new FRBs, while monitoring and follow-up observations with a steerable radio telescope such as the GMRT can break the degeneracy between the intrinsic period and an alias caused by the regular exposure pattern of CHIME.

Further sensitive observations such as these will be key to detecting any underlying periodicity with a short time-scale, as we continue to detect bursts with short separations. We will continue to observe

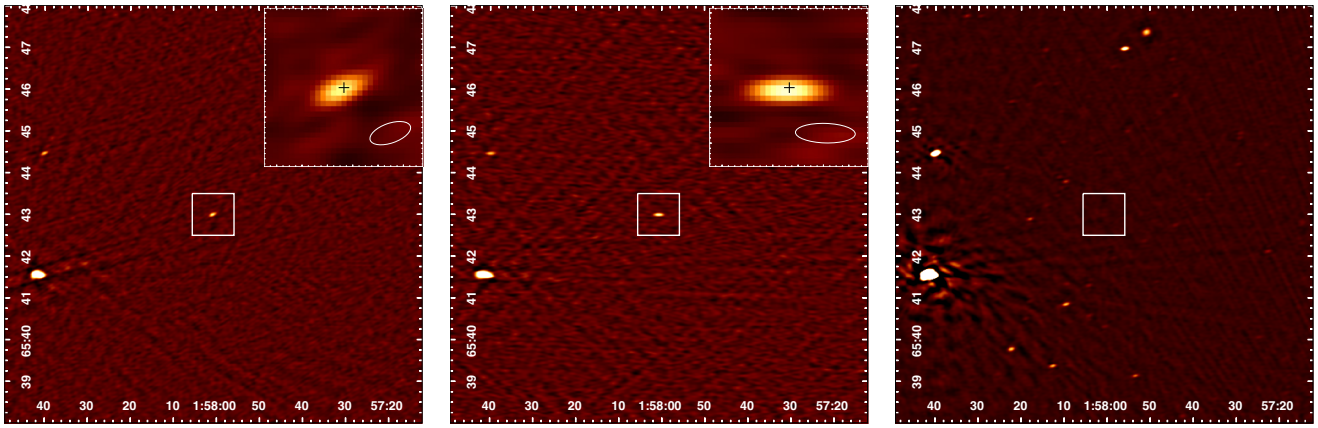

Figure 4. Images of 10×10 arcmin^2 region centred on the position of FRB 180916.J0158+65, which is indicated by the 1×1 arcmin^2 box. The left (burst 04) and middle (burst 11) plots show the detection of single bursts using visibilities from only two (burst 04) or one (burst 11) 2.68-s time samples. The inset of each plot shows the 1×1 arcmin^2 region around the burst. The CLEAN beam is shown in the bottom right of each inset and the EVN position is indicated by a black cross. The right plot shows a deep image made using data from the full ≈2-h observation of 2020 March 24.

during the active window to investigate the origin of the 16.35-d periodicity. For example, any modulation of the scintillation of the bursts as a function of the phase within the active window is evidence for orbital motion around a companion. Sensitive polarization observations in the future can help to constrain emission models and mechanisms.

We have imaged two of the brightest bursts with subarcsec precision, showing the promise of the GMRT to localize known repeating FRBs. The GMRT can also potentially localize newly detected repeating FRBs, especially as its field of view is well matched with the CHIME beam. While the time resolution of the uGMRT interferometer is currently limited to 670 ms, the increased sensitivity compared with CHIME will allow for imaging of the brighter CHIME bursts, above $\gtrsim 3$ Jy ms.

ACKNOWLEDGEMENTS

We thank the staff of the GMRT who have made these observations possible. GMRT is run by the National Centre for Radio Astrophysics of the Tata Institute of Fundamental Research. We acknowledge use of the CHIME/FRB Public Database, provided at https://www.chime-frb.ca/ by the CHIME/FRB Collaboration. We acknowledge the support of the Natural Sciences and Engineering Research Council of Canada (NSERC; funding reference number RGPIN-2019-067, CRD 523638-201). We receive support from the Ontario Research Fund - Research Excellence Program (ORF-RE), Canadian Institute for Advanced Research (CIFAR), Canadian Foundation for Innovation (CFI), Simons Foundation, Thoth Technology Inc. and Alexander von Humboldt Foundation. RSW acknowledges financial support from the European Research Council (ERC) for the ERC Synergy Grant BlackHoleCam under contract no. 610058. GMRT is run by the National Centre for Radio Astrophysics of the Tata Institute of Fundamental Research.

We acknowledge support of the Department of Atomic Energy, Government of India, under project no. 12-R&D-TFR-5.02-0700.

DATA AVAILABILITY

The data underlying this article will be shared on reasonable request to the corresponding authors.

REFERENCES

Aggarwal K., Law C. J., Burke-Spolaor S., Bower G., Butler B. J., Demorest P., Linford J., Lazio T. J. W., 2020, Research Notes of the American Astronomical Society, 4, 94
Amiri M.CHIME/FRB Collaboration et al. CHIME/FRB Collaboration), 2020, Nature, 582, 351
Andersen B. C., Ransom S. M., 2018, ApJ, 863, L13
Andersen B. C.CHIME/FRB Collaboration et al. CHIME/FRB Collaboration), 2019, ApJ, 885, L24
Andersen B. C.CHIME/FRB Collaboration et al. (CHIME/FRB Collaboration), 2020, preprint(arXiv:2005.10324)
Bannister K. W. et al., 2019, Science, 365, 565
Beniamini P., Wadiasingh Z., Metzger B. D., 2020, MNRAS, 496, 3390
Bochenek C. D., Ravi V., Belov K. V., Hallinan G., Kocz J., Kulkarni S. R., McKenna D. L., 2020, preprint(arXiv:2005.10828)
Chatterjee S. et al., 2017, Nature, 541, 58
Chawla P. et al., 2020, ApJ, 896, L41
Dai Z. G., Wang J. S., Wu X. F., Huang Y. F., 2016, ApJ, 829, 27
Gupta Y. et al., 2017, Current Science, 113, 707
Hessels J. W. T. et al., 2019, ApJ, 876, L23
Ioka K., Zhang B., 2020, ApJ, 893, L26
Levin Y., Beloborodov A. M., Bransgrove A., 2020, ApJ, 895, L30
Lorimer D. R., Bailes M., McLaughlin M. A., Narkevic D. J., Crawford F., 2007, Science, 318, 777
Lyutikov M., Barkov M. V., Giannios D., 2020, ApJ, 893, L39
McMullin J. P., Waters B., Schiebel D., Young W., Golap K., 2007, in Shaw R. A., Hill F., Bell D. J., eds, ASP Conf. Ser. Vol. 376, Astronomical Data Analysis Software and Systems XVI. Astron. Soc. Pac., San Francisco, CA, p. 127
Marcote B. et al., 2020, Nature, 577, 190
Pilia M. et al., 2020, ApJ, 896, L40
Prochaska J. X. et al., 2019, Science, 366, 231
Rajwade K. M. et al., 2020, MNRAS, 495, 3551
Ransom S. M., Eikenberry S. S., Middleditch J., 2002, AJ, 124, 1788
Ravi V. et al., 2019, Nature, 572, 352
Reddy S. H. et al., 2017, Journal of Astronomical Instrumentation, 6, 1641011
Sand K. R. et al., 2020, The Astronomer's Telegram, 13781, 1
Yang H., Zou Y-C., 2020, ApJ, 893, L31
Zanazzi J. J., Lai D., 2020, ApJ, 892, L15

This paper has been typeset from a TEX/LATEX file prepared by the author.